

# Construction of a Mitochondria-Endoplasmic Reticulum Dual-Targeted Red-Emitting Fluorescent Probe for Imaging Peroxynitrite in Living Cells and Zebrafish

Lingchao He,<sup>[a, b]</sup> Heng Liu,<sup>\*[b, c]</sup> Jinsheng Wu,<sup>[b]</sup> Ziyi Cheng,<sup>[b, c]</sup> and Fabiao Yu<sup>\*[a, b, c]</sup>

**Abstract:** Peroxynitrite (ONOO<sup>-</sup>) is one of the important reactive oxygen species, which plays a vital role in the physiological process of intracellular redox balance. Revealing the biological functions of ONOO<sup>-</sup> will contribute to further understanding of the oxidative process of organisms. In this work, we designed and synthesized a novel red-emitting fluorescent probe MCSA for the detection of ONOO<sup>-</sup>, which could rapidly respond to ONOO<sup>-</sup> within 250 s and exhibited high sensitivity to ONOO<sup>-</sup> with a low detection limit of

78 nM. Co-localization experiments demonstrated MCSA had the ability to localize into the mitochondria and endoplasmic reticulum. What's more, MCSA enabled monitoring ONOO<sup>-</sup> level changes during tunicamycin-induced endoplasmic reticulum stress. We have also successfully achieved the visual detection of exogenous and endogenous ONOO<sup>-</sup> in living cells and zebrafish. This work presented a chemical tool for imaging ONOO<sup>-</sup> in vitro and in vivo.

## Introduction

As one of the most important reactive oxygen species in cells, peroxynitrite (ONOO<sup>-</sup>) is produced by the rapid combination of nitric oxide and superoxide in organisms.<sup>[1]</sup> The main generating site of ONOO<sup>-</sup> is subcellular organelle mitochondria.<sup>[2]</sup> ONOO<sup>-</sup> has powerful oxidative and nitrative abilities, and can interact with various biomolecules such as lipids, nucleic acids and proteins, resulting in aberrant cell function, mitochondrial apoptosis and even cell necrosis.<sup>[3]</sup> ONOO<sup>-</sup> not only affects cell signaling transduction by nitrosating tyrosine residues, but also modulates intracellular redox balance by oxidizing protein cysteine residues.<sup>[4]</sup> Studies have shown that intracellular ONOO<sup>-</sup> can coordinate the immune system to defend against pathogens. The level fluctuations of ONOO<sup>-</sup> are closely related to the pathogenesis and progression of a variety of diseases, such as neurodegenerative diseases, cardiovascular diseases,

diabetes and cancer.<sup>[5]</sup> Therefore, it is vital to develop a rapid and efficient method for monitoring ONOO<sup>-</sup> in biological systems.

Under physiological conditions, ONOO<sup>-</sup> has a short lifetime (20 ms), high reactivity and low concentration (nanomolar level), so the detection of endogenous ONOO<sup>-</sup> is always a difficult issue. So far, there are electrochemical, UV-visible absorption spectroscopy and immunohistochemistry methods for the analysis of ONOO<sup>-</sup> concentrations, but none of these methods can be used for in situ imaging of ONOO<sup>-</sup> in vivo.<sup>[6]</sup> Very recently, fluorescence imaging technology based on fluorescent probes has become an ideal tool for exploring the physiological functions of ONOO<sup>-</sup> owing to its high temporal and spatial resolution, high sensitivity and non-invasiveness.<sup>[7]</sup> Depending on different types of reaction groups including double bond,<sup>[8]</sup> benzoborate ester,<sup>[9]</sup>  $\alpha$ -ketoamide,<sup>[10]</sup> indoline-2,3-dione,<sup>[11]</sup> trifluoromethyl ketone<sup>[12]</sup> and N-aminophenol,<sup>[13]</sup> a great deal of ONOO<sup>-</sup>-specific fluorescent probes have been reported. Although some fluorescent probes for imaging ONOO<sup>-</sup> have been designed, fluorescent probes with mitochondria and endoplasmic reticulum dual targeting were rare. In the meantime, there are few fluorescent probes to assess changes in ONOO<sup>-</sup> levels during endoplasmic reticulum stress.<sup>[14]</sup>

In this investigation, we disclosed a mitochondria-endoplasmic reticulum dual-targeted red-emitting fluorescent probe for detecting ONOO<sup>-</sup>. In an aqueous media under physiological pH, the probe MCSA could respond to ONOO<sup>-</sup> with marked fluorescence changes. Most importantly, MCSA enabled fluorescence imaging of ONOO<sup>-</sup> in mitochondria and endoplasmic reticulum of living cells and zebrafish. MCSA was capable of tracking ONOO<sup>-</sup> level fluctuations under the oxidative stress of endoplasmic reticulum.

[a] L. He, F. Yu

College of Chemistry and Chemical Engineering  
Qufu Normal University  
Qufu 273165 (P. R. China)  
E-mail: liuheng@hainmc.edu.cn  
yufabiao@hainmc.edu.cn

[b] L. He, H. Liu, J. Wu, Z. Cheng, F. Yu

Department of Radiotherapy  
Key Laboratory of Hainan Trauma and Disaster Rescue  
The First Affiliated Hospital of Hainan Medical University  
Hainan Medical University  
Haikou, 571199 (P. R. China)

[c] H. Liu, Z. Cheng, F. Yu

Key Laboratory of Emergency and Trauma  
Ministry of Education  
College of Emergency and Trauma  
Hainan Medical University  
Haikou 571199 (P. R. China)



Supporting information for this article is available on the WWW under <https://doi.org/10.1002/asia.202200388>



This manuscript is part of a special collection on Responsive Probes and Molecular Bioimaging.

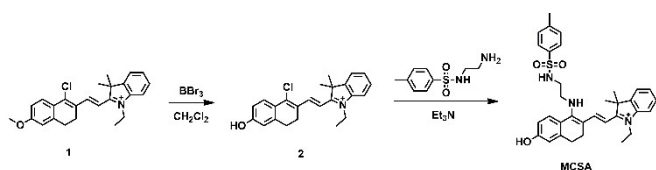
## Results and Discussion

### Design and synthesis of MCSA

In the design, MCSA was composed of dihydronaphthalene and hemicyanine (indolium iodide) skeletons. Indolium iodide conferred MCSA with good water solubility and mitochondria targeting ability, while N-(2-aminoethyl)-4-methyl-benzenesulfonamide conferred MCSA with endoplasmic reticulum targeting ability. The donor- $\pi$ -acceptor (D- $\pi$ -A) conjugated structure endowed MCSA with enhanced red-emitting properties. ONOO<sup>-</sup> could induce selectively oxidative cleavage of the double bond between dihydronaphthalene and indolium iodide, leading to significant changes in fluorescence. The synthetic procedure of MCSA was described in Scheme 1. Hemicyanine derivative underwent demethylation reaction with boron tribromide to afford fluorescent dye 2, followed by the nucleophilic substitution reaction with N-(2-aminoethyl)-4-methyl-benzenesulfonamide to give the probe MCSA. The chemical structure of MCSA was well characterized by nuclear magnetic resonance (NMR) and high-resolution mass spectrometry (HRMS). To confirm the ONOO<sup>-</sup>-induced oxidative reaction of MCSA, HRMS analysis was performed. The data showed that the peak at 402.9504 was assigned to the expected compound CA-COOH (Figure S5). The reaction mechanism was shown in Scheme S1.

### Fluorescence responses to ONOO<sup>-</sup>

MCSA was successfully prepared as illustrated in Scheme 1, and its spectral properties and analytical performance were investigated in detail in phosphate buffer solution (10 mM, pH 7.4). In the presence of ONOO<sup>-</sup>, MCSA displayed a maximum absorbance at 540 nm. However, after the addition of ONOO<sup>-</sup>, the absorbance blueshifted from 540 nm to 485 nm. Then the fluorescence responses of MCSA to ONOO<sup>-</sup> under the excitation at 520 nm were examined. The free MCSA emitted strong fluorescence and the maximum emission peak was located at 635 nm. As shown in Figure 1b, a dramatic decrease in fluorescence intensity with the continuous addition of ONOO<sup>-</sup> was observed, which was attributed to the destruction of the conjugated double bond in the backbone of MCSA. Before and after adding ONOO<sup>-</sup>, the fluorescence intensity of MCSA changed by approximately 9-fold. The fluorescence intensity at 635 nm of MCSA exhibited a good linear relationship with the addition of ONOO<sup>-</sup> (0 - 18  $\mu$ M), and the regression equation was  $F_{635nm} = -59.64 \times [\text{ONOO}^-] \mu\text{M} + 1214$  ( $R^2 = 0.9938$ ). The limit of detection for MCSA was found to be 78 nM (Figure 1c),



Scheme 1. Synthetic approaches to MCSA.

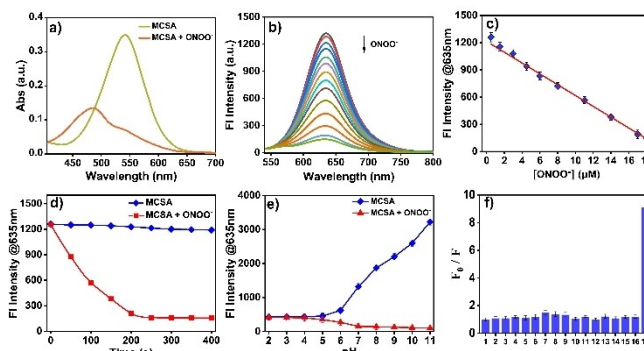


Figure 1. Spectral properties of MCSA. (a) Absorption spectra of MCSA before and after addition of ONOO<sup>-</sup> (18  $\mu$ M). (b) Fluorescence spectra of MCSA after the reaction with series concentrations of ONOO<sup>-</sup> (0–18  $\mu$ M). (c) The plot of the linear relationship between the relative fluorescence intensity at 635 nm of MCSA and concentrations of ONOO<sup>-</sup> (0–18  $\mu$ M). (d) Time-dependent fluorescence intensity of MCSA toward ONOO<sup>-</sup> (18  $\mu$ M). (e) Fluorescence intensity at 635 nm of MCSA with and without ONOO<sup>-</sup> (18  $\mu$ M) under different pH values. (f) Fluorescence responses of MCSA to different potential interfering species: 1. blank, 2. Na<sup>+</sup> (100  $\mu$ M), 3. Ca<sup>2+</sup> (100  $\mu$ M), 4. Zn<sup>2+</sup> (100  $\mu$ M), 5. Fe<sup>3+</sup> (20  $\mu$ M), 6. NO<sub>2</sub><sup>-</sup> (50  $\mu$ M), 7. NO (50  $\mu$ M), 8. NaClO (20  $\mu$ M), 9. H<sub>2</sub>O<sub>2</sub> (100  $\mu$ M), 10. O<sub>2</sub><sup>\*-</sup> (100  $\mu$ M), 11. -OH (50  $\mu$ M), 12. Na<sub>2</sub>S<sub>2</sub>O<sub>3</sub> (200  $\mu$ M), 13. <sup>1</sup>O<sub>2</sub> (50  $\mu$ M), 14. Citric acid (50  $\mu$ M), 15. Cys (500  $\mu$ M), 16. GSH (500  $\mu$ M), 17. ONOO<sup>-</sup> (18  $\mu$ M).

demonstrating MCSA was sensitive and potential for monitoring trace ONOO<sup>-</sup> in biological systems. Time-dependent fluorescence changes and pH effect of MCSA were studied. The fluorescence intensity of MCSA showed no obvious changes in the absence of ONOO<sup>-</sup>, and that of MCSA decreased rapidly upon treatment with ONOO<sup>-</sup>, reaching a plateau at 250 s (Figure 1d). MCSA emitted weak fluorescence in a pH range of 2.0–5.0, and the fluorescence suddenly increased when pH exceeded 6.0. MCSA exhibited significant fluorescence responses toward ONOO<sup>-</sup> under pH values between 6.0–11.0, indicating MCSA could be used in physiological pH 7.4 (Figure 1e). Subsequently, the influence of various biological analytes including ions (Na<sup>+</sup>, Ca<sup>2+</sup>, Zn<sup>2+</sup>, Fe<sup>3+</sup>, NO<sub>2</sub><sup>-</sup>), ROS/RNS (NO, ClO<sup>-</sup>, H<sub>2</sub>O<sub>2</sub>, O<sub>2</sub><sup>\*-</sup>, ·OH, <sup>1</sup>O<sub>2</sub>), RSS (Cys, GSH, Hcy) and others (S<sub>2</sub>O<sub>3</sub><sup>2-</sup>, citric acid), were evaluated (Figure 1f). The addition of other interfering species failed to induce apparent fluorescence changes of MCSA, while only ONOO<sup>-</sup> triggered a remarkable decrease in fluorescence. These results indicated MCSA possessed excellent spectroscopic properties and great potential for detecting ONOO<sup>-</sup> in complex systems.

### Fluorescence imaging of ONOO<sup>-</sup>

Given its excellent sensitivity and specificity for ONOO<sup>-</sup>, we set out to explore the application of MCSA in biological systems under confocal laser scanning microscopy. Before MCSA was subjected to fluorescence imaging, the cytotoxicity experiment using a standard CCK-8 assay was first performed to confirm the biocompatibility of MCSA. We chose three different cell lines (HeLa cells, Raw 246.7 cells, PC12 cells) to incubate with different concentrations of MCSA for 24 h. Clearly, the data in Figure S6 showed that MCSA was low toxic to the cells even the

concentration was 60  $\mu\text{M}$ . Next, we explored the imaging ability of MCSA for the detection of exogenous and endogenous  $\text{ONOO}^-$ . HeLa cells, Raw 246.7 cells and PC12 cells treated with MCSA displayed intense fluorescence signals respectively. In contrast, upon treatment with 0.5 mM SIN-1 (a commercial  $\text{ONOO}^-$  donor), the fluorescence signals of MCSA-loaded cells decreased to varying degrees, as illustrated in Figure 2.

Next, we investigated the ability of MCSA to image endogenous  $\text{ONOO}^-$  in living Raw 264.7 cells. The DAPI-loaded cells were first stimulated with LPS (1  $\mu\text{g}/\text{ml}$ ), IFN- $\gamma$  (60 ng/ml) for 4 h, 6 h, 8 h, then treated with PMA (10 nM) for 30 min. The cells were incubated with MCSA for 30 min before fluorescence imaging. As depicted in Figure 3a, b, the fluorescence intensities gradually decreased with the prolongation of stimulation time, suggesting the production of  $\text{ONOO}^-$  in cells. When the cells were treated with LPS/IFN- $\gamma$ /PMA and uric acid (UA, 100  $\mu\text{M}$ , a commercial  $\text{ONOO}^-$  scavenger) or aminoguanidine (AG, 1 mM, a nitric oxide synthase inhibitor), then incubated with MCSA, the fluorescence intensities were significantly restored compared with the group without inhibitor pretreatment (Figure 3c, d).

It has been widely reported that fluorescent probes linked to positive ion functional groups and N-(2-aminoethyl)-4-methyl-benzenesulfonamide can be selectively enriched in cellular

mitochondria and endoplasmic reticulum. To verify this, co-localization assays using two commercialized probes (ER-tracker red, Mito-tracker green) with MCSA were performed (Figure 4). The fluorescence of MCSA overlapped well with ER-tracker red, Mito-tracker green, and Pearson's co-localization coefficients were determined to be 0.83 and 0.94 respectively, indicating MCSA had the dual-targeting ability to the suborganelle mitochondria and endoplasmic reticulum.

### Imaging of $\text{ONOO}^-$ during ER stress

The endoplasmic reticulum is the central organelle for synthesis, dynamic folding and modification of protein. Endoplasmic reticulum homeostasis and concentration changes of calcium ion induces endoplasmic reticulum stress, which in turn promotes the production of  $\text{ONOO}^-$ . Tunicamycin (TM) is a well-known inducer of endoplasmic reticulum stress. HeLa cells were pretreated with TM (0, 1, 2, 3  $\mu\text{g}/\text{ml}$ ) for 8 h to induce different degrees of endoplasmic reticulum stress environment, followed by the incubation with MCSA for 30 min. As anticipated, the MCSA-treated group showed an intensive fluorescence signal, while the TM-treated group gradually weakened with the increasing TM concentrations (Figure 5).

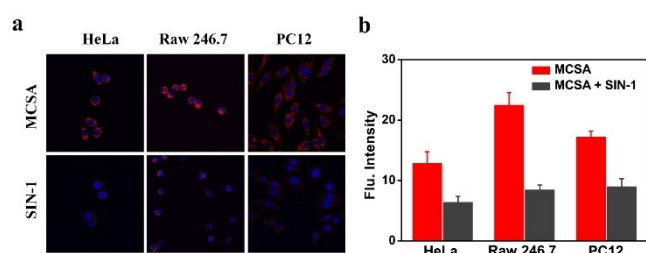


**Figure 2.** Imaging exogenous  $\text{ONOO}^-$  in different cells. (a) Confocal laser scanning microscopy of 10  $\mu\text{M}$  MCSA-loaded HeLa, Raw 246.7, PC12 cells only, or treated with SIN-1 (0.5 mM) for 30 min. The red channel was collected in the range of 600–700 nm ( $\lambda_{\text{ex}} = 514$  nm) and the DAPI channel was collected in the range of 415–550 nm ( $\lambda_{\text{ex}} = 405$  nm). (b) Relative red fluorescence intensities of MCSA labelled cells in (a) ( $n = 3$ ).

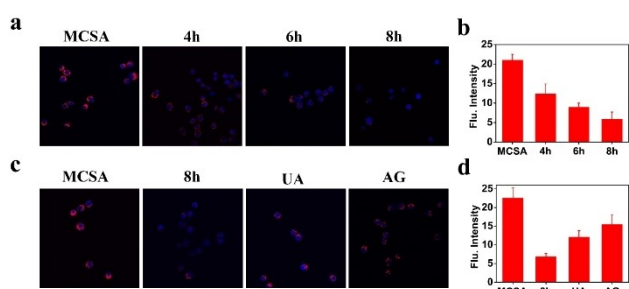


**Figure 3.** Imaging endogenous  $\text{ONOO}^-$  in Raw 264.7 cells. (a) The cells pretreated with LPS, IFN- $\gamma$  for 4 h, 6 h, 8 h, then PMA for 30 min, were incubated with MCSA (10  $\mu\text{M}$ ). (b) Relative red fluorescence intensities of MCSA labelled cells in (a) ( $n = 3$ ). (c) The cells were pretreated with LPS, IFN- $\gamma$  for 8 h, PMA for 30 min, UA or AG for 30 min, then incubated with MCSA for 30 min. (d) Relative red fluorescence intensities of MCSA labelled cells in (c) ( $n = 3$ ). The red channel was collected in the range of 600–700 nm ( $\lambda_{\text{ex}} = 514$  nm) and the DAPI channel was collected in the range of 415–550 nm ( $\lambda_{\text{ex}} = 405$  nm).

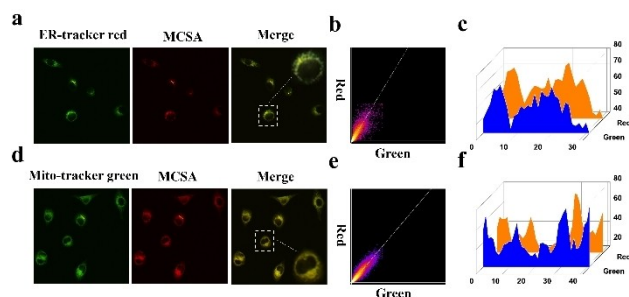


**Figure 4.** Co-localization of MCSA and ER-tracker red, Mito-tracker green in HeLa cells. The cells were co-incubated with MCSA (10  $\mu\text{M}$ ,  $\lambda_{\text{ex}} = 514$  nm,  $\lambda_{\text{em}} = 600$ –700 nm), and (a) ER-tracker red (500 nM,  $\lambda_{\text{ex}} = 561$  nm,  $\lambda_{\text{em}} = 580$ –600 nm); (d) Mito-tracker green (500 nM,  $\lambda_{\text{ex}} = 488$  nm,  $\lambda_{\text{em}} = 500$ –600 nm). (b, e) Intensity correlation plot of MCSA and ER-tracker red, Mito-tracker green. (c, f) Intensity 3D waterfall profiles of MCSA and ER-tracker red, Mito-tracker green within the linear ROI.

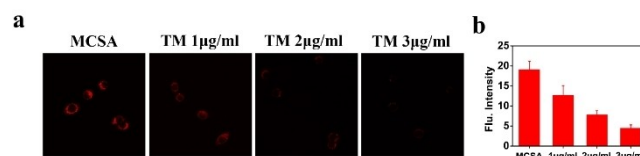


**Figure 5.** Imaging  $\text{ONOO}^-$  in HeLa cells during endoplasmic reticulum stress. (a) The cells pretreated with TM (0, 1, 2, 3  $\mu\text{g}/\text{ml}$ ) for 8 h, were incubated with MCSA (10  $\mu\text{M}$ ). (b) Relative fluorescence intensities of MCSA labelled cells in (a) ( $n = 3$ ).

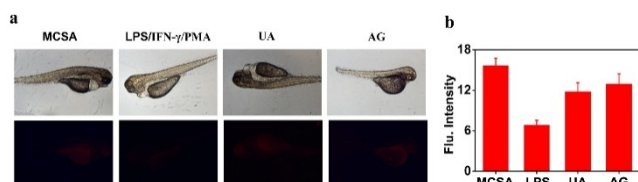


**Figure 6.** Imaging endogenous ONOO<sup>-</sup> in zebrafish. (a) The zebrafish were pretreated with LPS (2 μg/ml), IFN-γ (100 ng/ml), PMA (10 nM), UA (100 μM) or AG (1 mM) for 30 min, then incubated with MCSA for 30 min. (b) Relative red fluorescence intensities of MCSA labelled zebrafish in (a) (n = 3).

### Zebrafish imaging of ONOO<sup>-</sup>

To broaden the application of MCSA, we further explored the fluorescence imaging of MCSA in vivo using zebrafish as a model organism. It was found that the zebrafish loaded MCSA exhibited a bright fluorescence signal in Figure 6. When the zebrafish was successively stimulated by LPS/IFN-γ/PMA, and then incubated with MCSA, the fluorescence signal of zebrafish was significantly reduced, which was due to the production of ONOO<sup>-</sup>. By comparison, in the two groups of experiments with ONOO<sup>-</sup> inhibitors UA and AG, the dramatic elevation of fluorescence signals was observed. The results illustrated that MCSA was suitable for in vivo ONOO<sup>-</sup> imaging and ONOO<sup>-</sup> inhibitor screening.

### Conclusion

In summary, we have successfully constructed a red-emitting fluorescent probe MCSA for the detection of ONOO<sup>-</sup>, exhibiting fast response, high selectivity over other interfering species and sensitivity with a low detection limit in PBS buffer solution. Using MCSA, we have achieved that real-time visualization of exogenous ONOO<sup>-</sup> in different types of cell lines. Colocalization experiment results demonstrated that MCSA enabled selectively targeting intracellular mitochondria and endoplasmic reticulum. More importantly, MCSA was applicable for tracking level fluctuations of ONOO<sup>-</sup> during TM-induced endoplasmic reticulum stress. Moreover, MCSA could be applied for imaging endogenously produced ONOO<sup>-</sup> in zebrafish. Above all, we anticipate that MCSA can be used as a chemical tool to aid in the detection and treatment of ONOO<sup>-</sup>-related diseases.

### Experimental Section

**Synthesis and characterization of compound 2:** The mixture of compound 1 (260 mg, 0.5 mmol), boron tribromide (300 mg), dry dichloromethane (5 ml) was stirred at 0 °C. The reaction was monitored by TLC. After the reaction was completed, the mixture was poured into crushed ice, and extracted with dichloromethane. The organic phase was collected, and the solvent was removed by a rotary evaporator under reduced pressure. The mixture was purified on a chromatographic column with DCM/MeOH (v/v = 15:1), to give a purple-red solid. <sup>1</sup>H NMR (400 MHz, d<sub>6</sub>-DMSO): δ 10.57 (s, H), 8.49 (d, J = 15.7 Hz, 1H), 7.92 (d, J = 7.3 Hz, 1H), 7.88 (d, J = 7.8 Hz, 1H), 7.69 (d, J = 8.5 Hz, 1H), 7.66–7.61 (m, 2H), 7.16 (d, J =

15.7 Hz, 1H), 6.82–6.79 (m, 2H), 4.65 (q, J = 7.2 Hz, 2H), 2.91 (s, 4H), 1.76 (s, 6H), 1.44 (t, J = 7.2 Hz, 3H).

**Synthesis and characterization of MCSA:** The mixture of compound 2 (135 mg, 0.27 mmol), N-(2-aminoethyl)-4-methyl-benzenesulfonamide (285 mg, 1.35 mmol), dichloromethane (10 ml) was stirred at room temperature for 12 h. The reaction was monitored by TLC. After the reaction was completed, the solvent was removed by a rotary evaporator under reduced pressure, and the mixture was purified on a chromatographic column with DCM/MeOH (v/v = 15:1), to give a purple-red solid. <sup>1</sup>H NMR (400 MHz, CDCl<sub>3</sub>): δ 7.99 (d, J = 13.4 Hz, 1H), 7.85 (d, J = 8.4 Hz, 2H), 7.49 (d, J = 9.2 Hz, 1H), 7.47 (s, 1H), 7.36–7.29 (m, 4H), 7.17 (t, J = 7.6 Hz, 1H), 6.97 (d, J = 7.8 Hz, 1H), 6.63 (dd, J = 8.7, 2.4 Hz, 1H), 5.83 (d, J = 12.8 Hz, 1H), 4.06–3.96 (m, 4H), 3.76–3.72 (m, 1H), 3.65–3.60 (m, 1H), 3.28–3.26 (m, 2H), 2.98 (t, J = 6.2 Hz, 2H), 2.62 (t, J = 6.4 Hz, 2H), 2.40 (s, 3H), 1.74 (s, 6H), 1.42 (t, J = 6.7 Hz, 3H); <sup>13</sup>C NMR (100 MHz, CDCl<sub>3</sub>): δ 170.36, 165.43, 163.31, 146.61, 144.04, 143.41, 141.94, 140.79, 136.56, 129.76, 128.36, 128.24, 127.03, 123.79, 122.29, 119.68, 115.76, 115.61, 115.37, 108.94, 95.05, 67.37, 49.13, 48.44, 42.40, 29.64, 28.80, 24.97, 21.50, 11.79; HRMS m/z: C<sub>33</sub>H<sub>38</sub>N<sub>3</sub>O<sub>3</sub>S<sup>+</sup> [M-H]<sup>+</sup> calcd for 556.2628 found 556.2617.

### Acknowledgements

This work was supported by the Hainan Province Science and Technology Special Fund (ZDYF2021SHFZ219, ZDYF2021SHFZ245, ZDYF2020133), National Natural Science Foundation of China (21961010), Hainan Provincial Natural Science Foundation of China (820RC643), Natural Science Research Talent Project of Hainan Medical University (JBGS202101), and Hainan Province Clinical Medical Center (2021).

### Conflict of Interest

The authors declare no conflict of interest.

### Data Availability Statement

Research data are not shared.

**Keywords:** bioimaging · dual-targeted · fluorescent probe · peroxynitrite · red-emitting

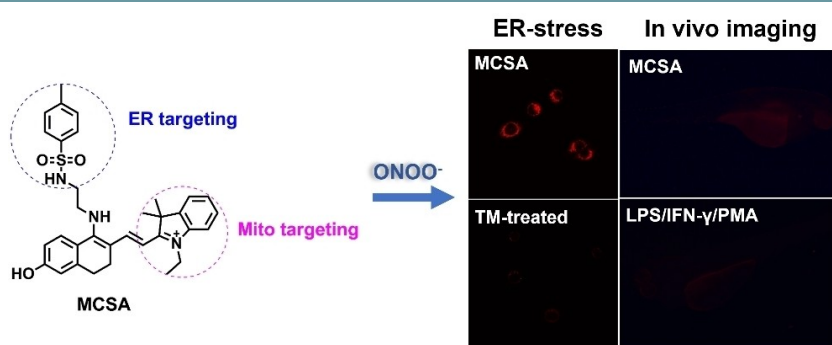
- [1] H. Sies, V. V. Belousov, N. S. Chandel, M. J. Davies, D. P. Jones, G. E. Mann, M. P. Murphy, M. Yamamoto, C. Winterbourn, *Nat. Rev. Mol. Cell Biol.* **2022**, <https://doi.org/10.1038/s41580-022-00456-z>.
- [2] a) J. Lee, C. H. Song, *Antioxidants* **2021**, *10*, 872; b) M. Ott, V. Gogvadze, S. Orrenius, B. Zhivotovsky, *Apoptosis*. **2007**, *12*, 913–922.
- [3] S. Bartesaghi, R. Radi, *Redox. Biol.* **2018**, *14*, 618–625.
- [4] a) H. Sies, D. P. Jones, *Nat. Rev. Mol. Cell Biol.* **2020**, *21*, 363–383; b) R. Radi, *Proc. Natl. Acad. Sci. USA* **2018**, *115*, 5839–5848.
- [5] a) F. Wang, Q. Yuan, F. Chen, J. Pang, C. Pan, F. Xu, Y. Chen, *Front. Cell. Dev. Biol.* **2021**, *9*, 742483; b) L. Liaudet, N. Rosenblatt-Velin, P. Pacher, *Curr. Vasc. Pharmacol.* **2013**, *11*, 196–207; c) M. Trujillo, G. Ferrer-Sueta, R. Radi, *Antioxid. Redox Signaling* **2008**, *10*, 1607–1620.
- [6] a) S. Zhao, G. Zang, Y. Zhang, H. Liu, N. Wang, S. Cai, C. Durkan, G. Xie, G. Wang, *Biosens. Bioelectron.* **2021**, *179*, 113052; b) M. Bandoowala, D. Thakkar, P. Sengupta, *Crit. Rev. Anal. Chem.* **2020**, *50*, 265–289; c) Z. Liu,

- C. Zhou, D. Liu, T. He, L. Guo, D. Xu, M. G. Kong, *AIP Adv.* **2019**, *9*, 015014.
- [7] a) Z. Mao, J. Xiong, P. Wang, J. An, F. Zhang, Z. Liu, J. Seung Kim, *Coord. Chem. Rev.* **2022**, *454*, 214356; b) D. Cheng, W. Xu, X. Gong, L. Yuan, X. B. Zhang, *Acco. Chem. Res.* **2021**, *54*, 403–415; c) L. Wu, A. C. Sedgwick, X. Sun, S. D. Bull, X. P. He, T. D. James, *Acc. Chem. Res.* **2019**, *52*, 2582–2597; d) S. Wang, L. Chen, P. Jangili, A. Sharma, W. Li, J. T. Hou, C. Qin, J. Yoon, J. S. Kim, *Coord. Chem. Rev.* **2018**, *374*, 36–54; e) Y. Zhou, W. Zhang, X. Wang, P. Li, B. Tang, *Chem. Asian J.* **2022**, e202200155; f) Y. Zhong, L. Yang, Y. Zhou, J. Peng, *Chem. Asian J.* **2022**, e202200038; g) X. Y. Song, R. Wang, J. Gao, X. Y. Han, J. Jin, C. J. Lv, F. B. Yu, *Chin. Chem. Lett.* **2022**, *33*, 1567–1571; h) J. T. Hou, K. K. Yu, K. Sunwoo, W. Y. Kim, S. Koo, J. Wang, W. X. Ren, S. Wang, X. Q. Yu, J. S. Kim, *Chem.* **2020**, *6*, 832–866.
- [8] a) R. Han, W. Shu, H. Kang, Q. Duan, X. Zhang, C. Liang, M. Gao, L. Xu, J. Jing, X. Zhang, *Anal. Chim. Acta* **2022**, *1203*, 339652; b) D. Ma, S. Hou, C. Bae, T. C. Pham, S. Lee, X. Zhou, *Chin. Chem. Lett.* **2021**, *32*, 3886–3889; c) J. Zhang, J. Kan, Y. Sun, M. Won, J. H. Kim, W. Zhang, J. Zhou, Z. Qian, J. S. Kim, *ACS Appl. Bio Mater.* **2021**, *4*, 2080–2088.
- [9] a) H. Kang, W. Shu, J. Yu, M. Gao, R. Han, J. Jing, R. Zhang, X. Zhang, *Sensor. Actuat. B* **2022**, *359*, 131393; b) Y. X. Ye, X. Y. Chen, Y. W. Yu, Q. Zhang, X. W. Wei, Z. C. Wang, B. Z. Wang, Q. C. Jiao, H. L. Zhu, *Analyst* **2021**, *146*, 6556–6565; c) Z. Wang, W. Wang, P. Wang, X. Song, Z. Mao, Z. Liu, *Anal. Chem.* **2021**, *93*, 3035–3041; d) M. Wang, C. Wang, W. Song, W. Zhong, T. Sun, J. Zhu, J. Wang, *Spectrochim. Acta Part A* **2021**, *251*, 119398.
- [10] a) X. Yin, W. Feng, S. Gong, G. Feng, *Dyes Pigm.* **2020**, *172*, 107820; b) W. Qu, C. Niu, X. Zhang, W. Chen, F. Yu, H. Liu, X. Zhang, S. Wang, *Talanta* **2019**, *197*, 431–435; c) J. B. Li, L. Chen, Q. Wang, H. W. Liu, X. X. Hu, L. Yuan, X. B. Zhang, *Anal. Chem.* **2018**, *90*, 4167–4173.
- [11] J. Cao, W. An, A. G. Reeves, A. R. Lippert, *Chem. Sci.* **2018**, *9*, 2552–2558.
- [12] a) J. Zhang, X. Zhen, J. Zeng, K. Pu, *Anal. Chem.* **2018**, *90*, 9301–9307; b) T. Peng, D. Yang, *Org. Lett.* **2010**, *12*, 4932–4935.
- [13] a) Q. Sun, J. Xu, C. Ji, M. S. S. Shaibani, Z. Li, K. Lim, C. Zhang, L. Li, Z. Liu, *Anal. Chem.* **2020**, *92*, 4038–4045; b) K. E. Knewton, D. Rane, B. R. Peterson, *ACS Chem. Biol.* **2018**, *13*, 2595–2602.
- [14] M. Yan, H. Fang, X. Wang, J. Xu, C. Zhang, L. Xu, L. Li, *Sensor. Actuat. B* **2021**, *328*, 129003.

---

Manuscript received: April 12, 2022  
 Revised manuscript received: April 28, 2022  
 Accepted manuscript online: May 6, 2022  
 Version of record online: ■■■, ■■■■

## RESEARCH ARTICLE



*L. He, H. Liu\*, J. Wu, Z. Cheng, F. Yu\**

1 – 6

**Construction of a Mitochondria-Endoplasmic Reticulum Dual-Targeted Red-Emitting Fluorescent Probe for Imaging Peroxynitrite in Living Cells and Zebrafish**



**A mitochondria-endoplasmic reticulum dual-targeted red-emitting fluorescent probe MCSA for imaging**

ONOO<sup>-</sup> in living cells and zebrafish has been designed and reported.